ADVANCED FUNCTIONAL MATERIALS

www.afm-journal.de

Enhanced Performance of P2-$Na_{0.66}(Mn_{0.54}Co_{0.13}Ni_{0.13})O_2$ Cathode for Sodium-Ion Batteries by Ultrathin Metal Oxide Coatings via Atomic Layer Deposition

Karthikeyan Kaliyappan, Jian Liu, Biwei Xiao, Andrew Lushington, Ruying Li, Tsun-Kong Sham, and Xueliang Sun**

Sodium-ion batteries are widely considered as promising energy storage systems for large-scale applications, but their relatively low energy density hinders further practical applications. Developing high-voltage cathode materials is an effective approach to increase the overall energy density of sodium-ion batteries. When cut-off voltage is elevated over 4.3 V, however, the cathode becomes extremely unstable due to structural transformations as well as metal dissolution into the electrolytes. In this work, the cyclic stability of P2-$Na_{0.66}(Mn_{0.54}Co_{0.13}Ni_{0.13})O_2$ (MCN) electrode at a cut-off voltage of 4.5 V is successfully improved by using ultrathin metal oxide surface coatings (Al_2O_3, ZrO_2, and TiO_2) deposited by an atomic layer deposition technique. The MCN electrode coated with the Al_2O_3 layer exhibits higher capacity retention among the MCN electrodes. Moreover, the rate performance of the MCN electrode is greatly improved by the metal oxide coatings in the order of $TiO_2 < Al_2O_3 < ZrO_2$, due to increased fracture toughness and electrical conductivity of the metal oxide coating layers. A ZrO_2-coated MCN electrode shows a discharge capacity of 83 mAh g^{-1} at 2.4 A g^{-1}, in comparison to 61 mAh g^{-1} for a pristine MCN electrode. Cyclic voltammetry and electrochemical impedance analysis disclose the reduced charge transfer resistance from 1421 to 760.2 Ω after cycles, suggesting that the metal oxide coating layer can effectively minimize the undesirable phase transition, buffer inherent stress and strain between the binder, cathode, and current collector, and avoid volumetric changes, thus increasing the cyclic stability of the MCN electrode.

1. Introduction

Recently, a great deal of research has been carried out to replace lithium-ion batteries (LIBs) containing toxic and expensive $LiCoO_2$ as an energy storage material for large-scale applications such as electrical vehicles (EV) and hybrid electrical vehicles (HEV).[1] Rechargeable sodium-ion batteries (RSBs) are considered as a promising alternative to LIBs along with almost same charge storage mechanism.[2] In addition, cathode materials for RSB can be fabricated from naturally abundant elemental Na.[2,3] Although both LIB and RSB have identical storage mechanism, the Na ion has a slightly larger ionic radius and a higher redox potential than Li.[4] Nevertheless, development of high power and energy density storage devices for EV and HEV from sustainable green materials (Na based cathodes) garners global attention.

The exploration of RSB began in the early 80s.[5,6] Numerous Na-based cathode materials with various structures have been reported, including layered metal oxides, olivine phosphates, NASICON, pyrophosphate, and fluorophosphates.[2,7–12] Among them, P2-type layered metal oxides were found to deliver high energy density, due to the high theoretical capacity, fast Na-ion diffusion rate, and reduced slab-gliding during charge–discharge (C/DC) cycling.[13,14] Furthermore, P2-layered oxide with multitransition metals showed enhanced electrochemical performance compared to their parent components, such as $NaMO_2$ (M = Ni, Mn, Cr, Co, and Fe).[2,3,5,7,13–15] So far, $Na(Mn_{1/3}Ni_{1/3}Fe_{1/3})_2$, $NaMO_2$ (M = Cr, Fe, Co, and Ni), $Na_{0.67}Mn_{0.65}Fe_{0.2}Ni_{0.15}O_2$, $Na_{0.67}(Mn_{0.65}Co_{0.2}Ni_{0.15})O_2$, $Na_{2/3}Ni_{1/3}Mn_{2/3-x}Ti_xO_2$, $Na_{2/3}(Ni_{1/3}Mn_{2/3})O_2$, $Na_{2/3}(Mn_{1/2}Fe_{1/2})O_2$, $Na(Mn_{1/3}Ni_{1/3}Co_{1/3})_2$, and $Na_{0.67}Mn_{1-x}Mg_xO_2$ have been identified as potential candidates for cathode materials in RSB.[2–4,6,8,10,13,14,16,17] All these materials are known to exhibit large capacities as well as stable cycle life at cut-off voltages below 4.25 V.[2,3,5,7,13–16,18] However, many of these materials experience severe capacity decay during charge–discharge cycling at cut-off voltages above 4.3 V.[18,19] The capacity fading

Dr. K. Kaliyappan, Dr. J. Liu, Dr. B. Xiao, A. Lushington, R. Li, Prof. X. Sun
Department of Mechanical and Materials Engineering
University of Western Ontario
London, Ontario N6A 5B9, Canada
E-mail: karthik506@gmail.com; xsun9@uwo.ca
Dr. J. Liu
School of Engineering
University of British Columbia
Kelowna, British Columbia V1V 1V7, Canada
Dr. T.-K. Sham
Department of Chemistry
University of Western Ontario
London, Ontario N6A 5B7, Canada

DOI: 10.1002/adfm.201701870

during high-voltage operation mainly arises from structural transformations as well as metal dissolution into the acidic electrolyte. These issues severely restrict P2-type materials for use in high power applications.[18,20] There are a few of reports investigating the electrochemical performance of P2-type layered materials cycled above 4.45 V. Wang et al. reported that P2-$Na_{2/3}[Ni_{1/3}Mn_{2/3}]O_2$ material could deliver a capacity of ≈140 mAh g^{-1} at 0.1 C rate between 2.0 and 4.5 V, and retain ≈29% of its capacity in the following 100 cycles.[18] Lu et al. achieved a discharge capacity of 161 mAh g^{-1} for P2 $Na_{2/3}[Ni_{1/3}Mn_{2/3}]O_2$ using a low current rate of C/85 within a voltage window of 2–4.5 V.[20] However, all these studies were unable to achieve stable cycling behavior for P2-type layered materials under high voltage charge–discharge conditions. It has been reported that the use of a conductive carbon/metal oxide coating on the cathode surface could effectively prevent metal dissolution and increase conductivity, thereby enhancing cycling stability.[11,21] In spite of increasing the conductivity and rate performance of RSB cathodes, carbon coating has a number of drawbacks such as, decreased initial capacity due to the presence inactive carbon on the surface.[22] Instead, metal oxide coatings not only help to protect the active species from dissolving into the electrolyte but also increase the capacity.[23,24] Although performance enhancement of RSB cathode by carbon coating was reported by several groups, no literature can be found about the utilization of metal oxide coatings to improve the reversibility of RSB cathodes.[2,3,11] For this reason, we are adopting metal oxide coatings for the first time to enhance the cyclic stability of P2-$Na_{0.66}(Mn_{0.54}Co_{0.13}Ni_{0.13})O_2$ (MCN) cycled within 2–4.5 V.

Recently, atomic layer deposition (ALD) has been considered as a favorable technique to obtain uniform metal oxide coatings, which can be hardly achieved by conventional coating methods like sol–gel and hydrothermal method, on a number of electrode materials.[23] ALD has been used to improve the overall cell performance of various energy storage devices including LIBs, lithium–sulfur batteries, and fuel cells.[4,23–28] Nevertheless, the effective application of ALD in RSB is limited. The first report of Al_2O_3 ALD deposition on a tin anode for RSB application was demonstrated by Han et al.[29,30] Additionally, it was also reported by other groups that metal oxides coated with 2 ALD cycles were optimal for improving capacity and cyclic stability.[25,26,30,31] In spite of increased structural stability from thicker coatings (5, 10, or 20 ALD cycles), increased thickness was found to hinder the active species from participating in the electrochemical reactions.[24,26,27,30,31] In this regard, different metal oxide coatings (Al_2O_3, ZrO_2, and TiO_2) with 2 cycles of ALD was performed on the MCN electrode herein. Their influence on charge–discharge behaviors at different current densities was investigated in detail. Furthermore, the investigation of metal oxide coating on RSB cathode may lead to the fabrication of high efficient energy storage devices for large-scale application in the near future.

2. Result and Discussion

The X-ray powder diffraction (XRD) patterns of pristine and MCN powders coated with different metal oxides are shown in **Figure 1**a. The XRD patterns demonstrate a P2-type hexagonal structure with a $P6_3/mmc$ space group (JCPDS PDF No. 194).[13,14,16] The XRD patterns obtained for MCN powders also display intense peaks with no impurity phases detected, confirming the formation of highly crystalline MCN flakes using the citric-acid-assisted sol–gel method. Additionally, diffraction peaks associated with Al_2O_3, ZrO_2, and TiO_2 cannot be observed in the XRD patterns of MCN–Al, MCN–Zr, and MCN–Ti, respectively. This is due to the ultrathin coating thickness of the metal oxides as well as their amorphous nature.[26,27] The calculated lattice parameter values are identical for the pristine and MCN powders and the coated metal oxide coated ones (as shown in Figure 1a). Figure 1b presents the surface morphology of MCN powders prepared at 850 °C for 12 h. Clearly, the chelating agent (citric acid) leads to the formation of MCN microflakes with uniform particle size and distribution.[32] The stoichiometry of MCN powders was determined using inductively coupled plasma analysis. The atomic ratio of Na, Mn, Ni, and Co in MCN was measured to be ≈0.59, 0.562, 0.121, 0.119, respectively, which is in good agreement with the theoretical values. In addition, it was reported that the cathode prepared with off-stoichiometric ratio exhibited better electrochemical stability than that of conventional stoichiometry cathodes.[32] Thus, a better electrochemical behavior could be expected from pristine MCN powders.[17,32,33] Further, Ni, Mn, and Co in MCN would have the valence state of 2+, 4+, and 3+, respectively, which will be confirmed in cyclic voltammetry (CV) and charge–discharge experiments.

An average particle size of ≈1.5 µm can be observed for the active microflakes. Moreover, the surface and edges of MCN are smooth and do not show any agglomeration even after high temperature calcination. It is well known that materials prepared with uniform particle distribution can deliver enhanced charge storage characteristics due to their ability to propagate ionic/electronic diffusion.[32,33] Conversely, the surface of MCN particles was found to become rough after deposition of metal oxides by ALD, as presented in Figure S1 (Supporting Information).[24,25,27] Since the measurement of coating thickness for 2 ALD cycles is too difficult, we conducted experiments using 10 ALD cycles of Al_2O_3 to determine the coating thickness. Figure 1c illustrates the high-resolution transmission electron microscope (HR-TEM) image of 10 cycles of amorphous Al_2O_3 coated MCN particles and the coating thickness can be measured as ≈1.5 nm with uniform deposition.[23,26–28,53] In our previous work, we have reported that the growth rate of TiO_2 and ZrO_2 per ALD cycle was about 0.12 and 0.13 nm per cycle, which equals the coating thickness of 1.2 and 1.3 nm, respectively, for TiO_2 and ZrO_2 in 10 ALD cycles.[27,31] In addition, the uniformity of metal ions and coating material distribution on MNC powder was examined using energy-dispersive X-ray spectroscopy (EDX) and their corresponding EDX mapping are presented in Figures S2–S5 (Supporting Information). Figure S2 (Supporting Information) reveals that the atomic level mixing of Mn, Ni, Co, and Na ions with similar intensities. In addition, the uniform distribution of coating materials on the surface of the MCN powder is also confirmed in Figures S3–S5 (Supporting Information). This is demonstrated that the ALD is capable of depositing ultrathin uniform metal oxide coating on the surface of both powder and electrode.[27,28,31]

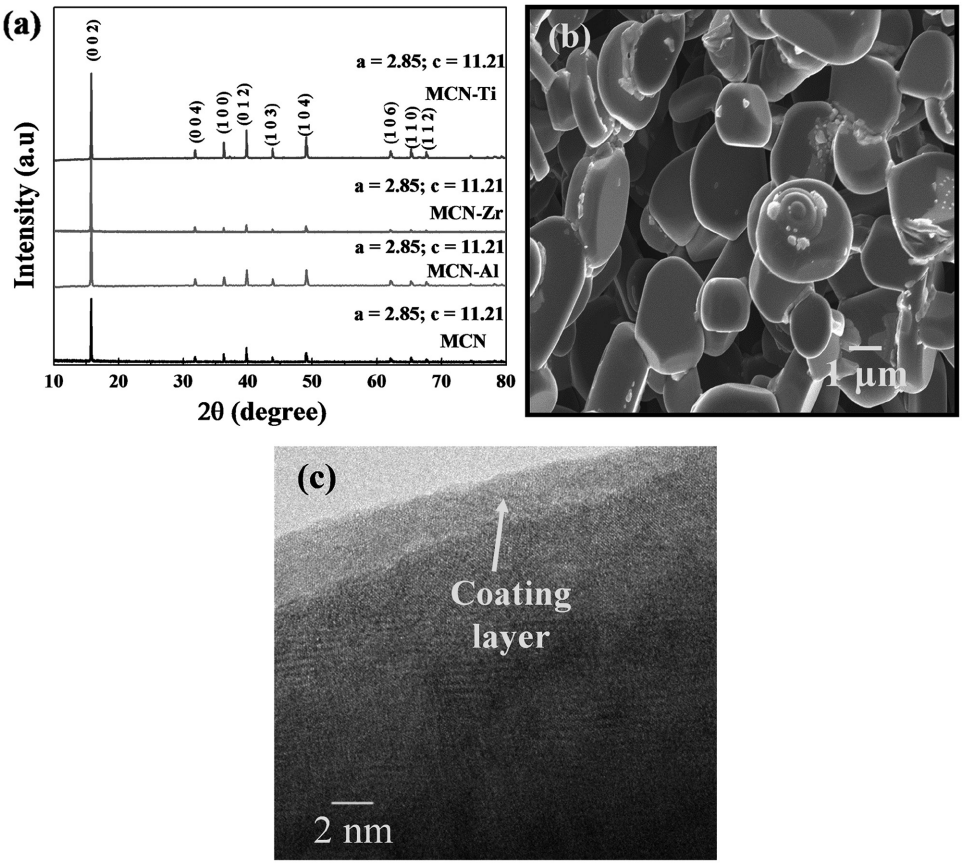

Figure 1. a) XRD patterns of the pristine MCN and the MCN electrodes coated with different metal oxides by ALD. b) SEM of MCN microflakes and c) HR-TEM of a MCN particle with 10 ALD cycles of Al_2O_3 coating layer.

The presence of various metal oxide coating layers on the surface are further confirmed through X-ray photoelectron spectroscopy (XPS) analysis with the corresponding spectra given in **Figure 2**. Representative peaks for Al 2p, Zr 4p, and Ti 3p can be detected at ≈74.5, 31.9, and 32.6 eV for MCN–Al, MCN–Zr, and MCN–Ti samples, respectively, revealing the existence of Al_2O_3, ZrO_2, and TiO_2 coatings on MCN electrode surface.[26,34,35]

Charge–discharge curves of pristine and MCN electrodes coated with different metal oxides are presented in **Figure 3**a. The charge–discharge profiles are taken between 2 and 4.5 V at a current density of 0.16 A g^{-1}. All curves display three clear plateaus during the charge and discharge process. During charging, the curves exhibit plateaus around ≈4.3, 3.6, and 2.3 V, which can be related to the electrochemical oxidation reactions of $Ni^{2+/4+}$, $Co^{3+/4+}$, and $Mn^{3+/4+}$, respectively.[36] The corresponding reduction plateaus are also observed at respective positions during the discharge process. However, the MCN–Ti cell demonstrates a shorter Ni oxidation and reduction plateau, which is deleterious for achieving high capacity.[37] Furthermore, MCN–Ti electrode also has a slightly higher charge voltage platform and lower discharge plateau, indicating the presence of higher polarization and reduced initial capacity value.[38] The initial discharge capacities of ≈121, 123, 122, and 106 mAh g^{-1} are obtained from MCN, MCN–Al, MCN–Zr, and MCN–Ti electrodes, respectively, at a current density of 0.16 A g^{-1}. Pristine and MCN coated with Al_2O_3 and ZrO_2 thin film exhibit similar discharge capacity, while MCN with TiO_2 layer delivers the lowest one.[39] It was reported that cathode materials coated with TiO_2 displayed a lower capacity value

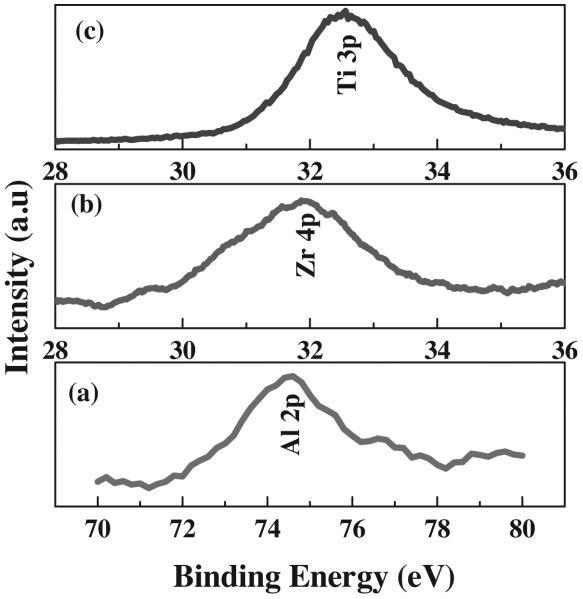

Figure 2. XPS of a) Al 2p, b) Zr 4p, and c) Ti 3p peaks of Al_2O_3, ZrO_2, and TiO_2 coating on MCN electrode.

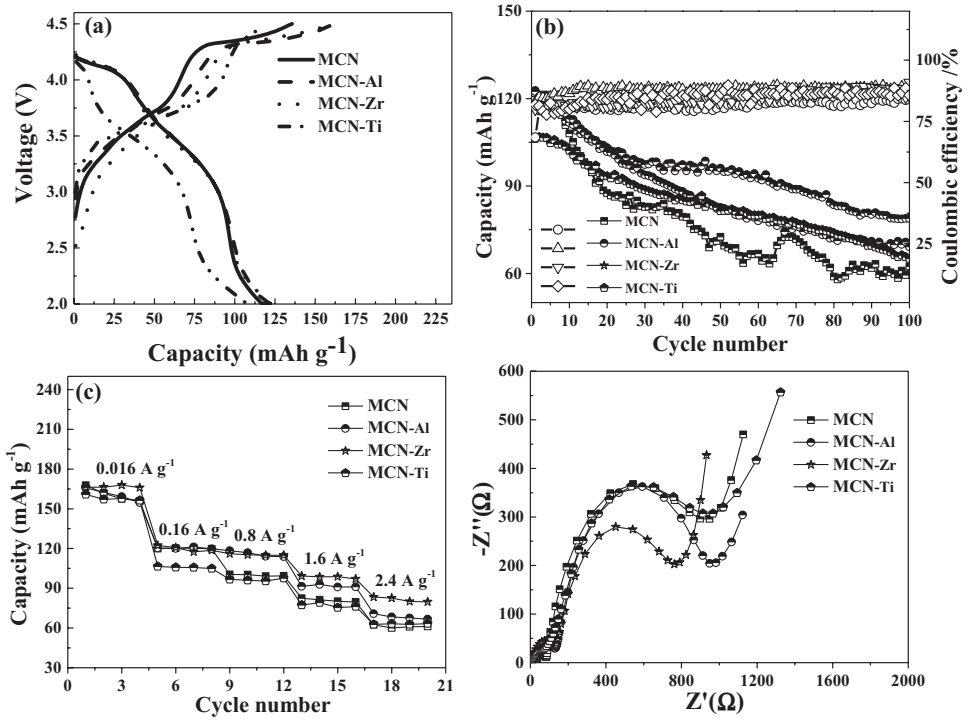

Figure 3. a) Charge–discharge profiles and b) cycle life of pristine and MCN electrode with metal oxide coatings at 0.16 A g^{-1} (1 C rate) current density within 2–4.5 V. c) Rate capability of the electrodes at different current densities and d) Nyquist plots of MCN and MCN coated with different metal oxides recorded at open circuit voltage.

when the cut-off voltage is increased above 4.4 V due to the catalytic activity of TiO_2.[37,39–42] Zheng et al. reported that using an increased cut-off voltage results in the decomposition of electrolyte catalyzed by TiO_2, thereby delivering diminished electrochemical activity.[40]

The cycling performances of the cells recorded at a current density of 0.16 A g^{-1} are presented in Figure 3b. The pristine MCN electrode has poor cycling stability along with a capacity of ≈121 mAh g^{-1} and maintains only 50% of its initial value after 100 cycles. Despite displaying a monotonous capacity fading, the cyclic stability for MCN in the present investigation still outperforms P2-type cathode materials cycled about 4.4 V in previous studies.[18,19] This enhanced behavior found for pristine MCN electrode may stem from its uniform particle size and even distribution, resulting in shortened Na ion diffusion length, enabling better contact between active particles, and thus resulting in enhanced electrochemical Na-ion storage performance.[32,33] The cyclic performance of MCN electrode can be further improved through the use of ALD metal oxide coatings. Among the three metal oxide coatings, MCN–Al electrode demonstrates improved cyclic stability, while MCN–Ti electrode shows poor cyclic behavior. Similar phenomenon has been reported in $LiCoO_2$ electrode coated with different metal oxide layers.[27] Although the initial capacity of MCN–Ti electrode is lower than the pristine MCN electrode, its cyclic stability is improved.[38,40] The enhanced cyclic stability of MCN covered with Al_2O_3 is mainly associated to the difference in band gap energies (E_g) between the MCN and coated materials.

Previous reports have indicated that the electrons in the conduction band of cathode materials move into the coating materials and undergo a redox reaction, if the E_g difference between the electrode and coating material is relatively small.[42,43] Here, the E_g of Al_2O_3, ZrO_2, and TiO_2 is about 9.00, 5.80, and 3.18 eV, respectively.[42,43] Hence, enhanced cyclic stability can be obtained from MCN–Al electrode. In contrast, the rate performance of the cells is mainly influenced by the conductive nature and mechanical integrity of the coating layer.[39] Besides, metal oxide coating layer on the surface was provided a flexible structure against the mechanical strain and stress formed during the cycling process, which causes the poor electrochemical behavior.[27,31]

Figure 3c illustrates the rate performance of the cells cycled at different current densities from 0.016 to 2.4 A g^{-1} within 2–4.5 V. It is well known that electrode material experiences high stress change during charge–discharge processes at high current densities. Therefore, a coating layer with high fracture toughness is necessary to attain high rate performance of cathode.[44] Previous reports have shown that ZrO_2 coating has a higher fracture toughness value (12 mPa m^{-2}) than Al_2O_3 (3.5 mPa m^{-2}), B_2O_3, TiO_2, and SiO_2.[29] As seen from Figure 3c, the discharge capacity of all samples linearly decreases with increasing current density as a result of polarization. MCN–Zr displays the best rate performance among all cells tested. Even at a high current density of 2.4 A g^{-1} (15 C), the cell made from MCN–Zr electrode delivers a capacity of ≈83 mAh g^{-1}, which is the highest value for sodium based P2-type layered materials, to the best of our knowledge.[2,3,10,13,14,19,20,45] The rate performance of various known Na-ion cathodes are compared with MCN–Zr electrode and presented in Figure S2 (Supporting Information). Figure S6 (Supporting Information) reveals that the MCN–Zr delivered one of the best rate performance compared to other

layered Na based intercalation cathodes reported in literatures.[2,3,31] It is therefore concluded that ultrathin ZrO_2 layer on MCN helps buffer the mechanical stress induced during charge/discharge process, retains the structural integration and electrochemical behavior, especially at high voltage.[44] Hence, enhanced rate performance is realized in MCN–Zr cell than other metal-oxide-coated electrodes.[27,31,41,44] Conversely, MCN–Ti delivers poor rate capability than other metal-oxide-coated electrodes, due to the low toughness of TiO_2 coating, consistent with previous reports.[37,39]

The effect of the ALD coating layers on the conductive profile is studied using electrochemical impedance spectroscopy (EIS) measurements and the Nyquist plots, as given in Figure 3d. All EIS plots consist of a semicircle in high frequency region associated to the solution resistance (R_s), and another semicircle in the low frequency region, corresponding to charge transfer resistance (R_{ct}). The former can be assigned to the Na-ion migration through the coating layer and the latter can be attributed to the resistance between the cathode–electrolyte interface.[27] The electrodes with different metal oxide coatings exhibit different R_s values due to the different nature of the coating layer. As seen from Figure 3d, R_s value of ≈48.3, 132.8, 139.5, 141.2 Ω can be calculated for MCN, MCN–Al, MCN–Zr, and MCN–Ti, respectively. The R_s of pristine MCN is smaller than that of metal oxide coated MCN electrodes, indicating that the metal oxide coating alleviates the formation of stable solid-electrolyte interfacial layer for charge–discharge studies.[27,35,41] On the other hand, a large difference in R_{ct} can be observed from Figure 3d. Among the cells, MCN–Zr shows a lower R_{ct} of ≈760.2 Ω, while MCN–Al cell exhibits an R_{ct} of ≈961.8 Ω at open circuit voltage, due to the low conductivity of Al_2O_3 layer. However, the MCN and MCN–Ti electrodes have larger R_{ct} values. The results obtained from EIS measurement correlate well with the rate performance studies in which enhanced rate performance is noted for MCN electrodes coated with ZrO_2 layer, whereas MCN with TiO_2 layer demonstrate diminished rate performance. The low rate performance of MCN–Ti electrode could be a result of high catalytic activity of TiO_2.[37,39,41]

X-ray absorption fine structure (XAFS) analysis was carried out to reveal the changes of local chemical structure around the Co, Mn, and Ni atoms in MCN electrodes after electrochemical cycling at 1 C for 100 cycles as shown in **Figure 4**a–c. All spectra are compared to a standard, commercial $Li(Ni_{1/3}Mn_{1/3}Co_{1/3})O_2$ (NMC) spectra with known K-edges. All spectra display a pre-edge absorption peak, which can be assigned to the electronic excitation of 1s core levels to a 3d unoccupied orbital. This weak peak is also attributed to 3d–4p orbital mixing, resulting from the distorted octahedral 3a site in the rhombohedral R3m space group.[46]

The main absorption peaks at high energy in all spectrums are due to the dipole transitions from 1s core electrons to unoccupied 4p orbitals. The peak position of Co K-edge spectrum for all samples in Figure 4a remains unchanged and almost identical to the Co^{3+} reference spectrum of standard NMC powders. This demonstrates that the local ionic state around the Co atom of all coated and pristine MCN samples is not significantly affected and primarily exists in the 3+ oxidation state.[47] Similarly, Mn K-edge spectra of MCN electrodes with and without coatings in Figure 4b does not exhibit energy shifts, representing that most of Mn atoms in MCN samples are in Mn^{4+} state (it is important to discuss this, because CV curves do show three reduction/oxidation peaks associated with $Ni^{2+/4+}$, $Co^{3+/4+}$, and $Mn^{3+/4+}$).[47,48] In contrast, the Ni K-edge of pristine MCN and MCN–Ti electrodes demonstrate a rigid edge shift toward higher energy compared to the standard NMC K-edge spectrum. This energy shift toward higher energy suggests that the oxidation state of Ni in MCN and MCN–Ti electrodes could not retain its 2+ state following charging–discharging at 1 C

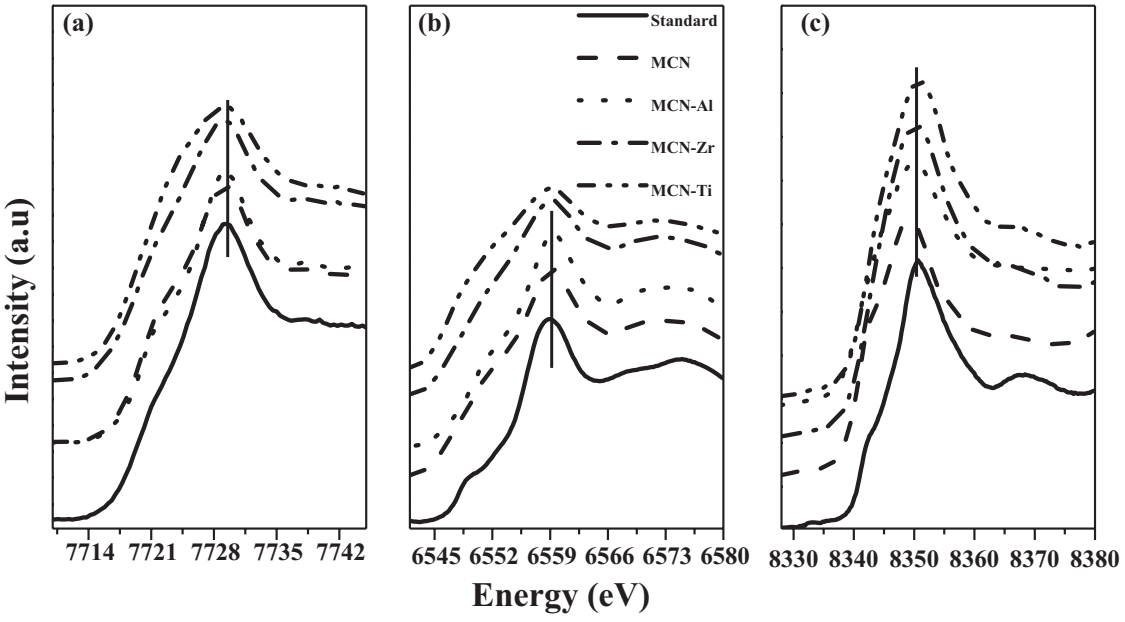

Figure 4. a) Co K-edge, b) Mn K-edge, and c) Ni K-edge spectra of pristine and metal-oxide-coated MCN electrodes recorded after 100 charge–discharge cycles at 1 C rate.

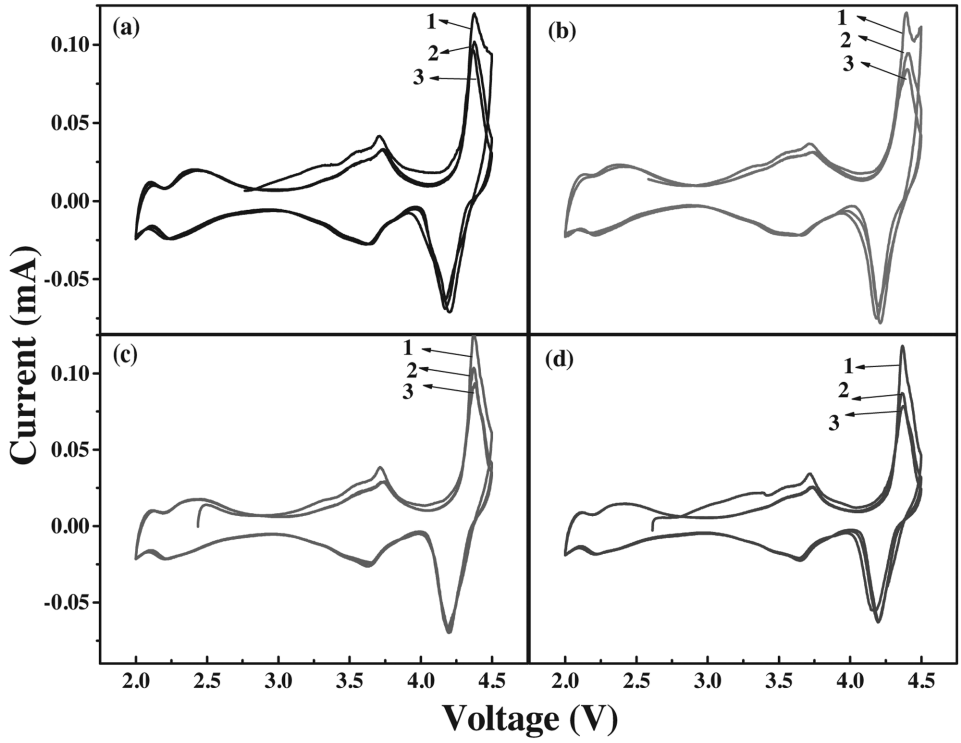

Figure 5. CV curves of a) MCN, b) MCN–Al, c) MCN–Zr, (d) MCN–Ti electrodes between 2 and 4.5 V at 0.1 mV s^{-1} scan rate for 3 cycles.

rate for 100 cycles. The XAFS results demonstrate that pristine MCN and MCN–Ti electrodes exhibited the lowest discharge capacity retention due to the variation in initial oxidation state of Ni ions following electrochemical cycling, resulting in the a reduction of $Ni^{2+/4+}$ redox reactions during the charging and discharging process.[46] Among the metal oxide coated MCN electrodes, the peak position of MCN–Al and MCN–Zr electrodes are unchanged and similar to the standard NMC Ni K-edge spectra, demonstrating that the oxidation states of Ni-ions are in Ni^{2+} state and the redox reaction of $Ni^{2+/4+}$ couple is completely reversible. Moreover, a slight increase in the pre-edge peak intensity of pristine MCN and MCN–Ti spectrum are also observed in Figure 4c. It could be attributable to increased local structural distortion of the Ni-O_6 octahedra due to the increased amount of Jahn–Teller active Ni^{3+} ions.[46–48] This discloses that MCN coated with Al_2O_3 and ZrO_2 layer should exhibit enhanced electrochemical behavior than that of uncoated sample. The outcome of XAFS studies correlated well with the results obtained from C/DC studies.

CV traces, given in **Figure 5**, presents useful information regarding the electrochemical behavior of the electrodes coated with different metal oxides. The CV curves are measured between 2 and 4.5 V at 0.1 mV s^{-1} for 3 cycles. The CV curves display three redox peaks during the positive and negative scans, confirming the complex Na-ion storage mechanism into the structure.[49]

Ma et al. described this storage mechanism of P2-type cathodes as a phenomenon related to the Na-ion vacancy ordering and gliding of oxygen planes.[49,50] The redox peaks noted at ≈2.3, 3.6, and 4.3 V represent the oxidation/reduction reaction of $Mn^{3+/4+}$, $Co^{3+/4+}$, and $Ni^{2+/4+}$, respectively.[51,52] As seen in Figure 4, metal oxide coated MCN electrodes, especially with Al_2O_3 and ZrO_2, show strong current responses compared to pristine MCN electrodes. This confirms the improved reaction kinetics of MCN electrode by various metal oxide coatings.[27,41] Additionally, MCN–Al cell has the highest current response, demonstrating a high capacity value of the cell. Moreover, a small peak shift toward lower potential range during reversal scans is detected for MCN–Ti cell, representing the lower electrochemical polarization of Ni^{2+}/Ni^{4+} redox couple reaction.[37,39,41] This restricts the Ni^{2+}/Ni^{4+} couple to be participated in the electrochemical Na-ion storage reaction and decreases the initial capacity values, which agree well with the charge–discharge and rate performance studies. The higher current response of Al_2O_3 and ZrO_2 coated MCN electrodes are attributed to high E_g values as well as from improved conductive profile through coating effect as confirmed using EIS measurements in Figure 2d.[24,27,29,37,41]

3. Conclusion

Significant performance improvement of MCN has been achieved by using various metal oxide coatings deposited by ALD technique. The charge–discharge behavior of the electrodes was mainly influenced by the nature of the metal oxide coatings. The MCN electrode coated with ultrathin Al_2O_3 (2 cycles of ALD) layer exhibited the best cyclic stability, while MCN with ZrO_2 coating delivered the highest rate performance. The enhanced cyclic performance of Al_2O_3 coated electrode was associated to its high band gap energy (9.00 eV) as compared to ZrO_2 (5.8 eV) and TiO_2 (3.18 eV). The high rate performance of

ZrO_2 coated MCN electrode would result from its high fracture toughness. In contrast, MCN with TiO_2 coating displayed poor Na-ion storage behavior than Al_2O_3 and ZrO_2 coated ones, due to the high catalytic activity of coating layer, which decreased its capacity value. As a result, coating ultrathin metal oxide layers on electrodes by ALD is a promising approach to fabricate high performance sodium-ion batteries for future applications.

4. Experimental Section

Citric-acid-assisted sol–gel method was used to prepare MCN microflakes. Citric acid serves as a chelating agent to minimize the agglomeration of MCN particles during high temperature calcination. In a typical synthesis process, appropriate amount of Na, Mn, Ni, and Co acetates were dissolved in 50 mL of distilled water. Then, 50 mL of aqueous citric acid was added into the above solution and stirred at 110 °C until a viscous solution formed. This solution was calcined first at 400 °C for 4 h and then at 850 °C for 12 h in air.

ALD Coating of Different Metal Oxides: The ALD of metal oxides is more effective when it was done on electrode surface instead of coating on as prepared powder as the inherent electronic properties of metal oxide altered the ionic and electronic transportation.[27,31] Thus, the ALD was employed on the surface of the electrode. The electrodes used for ALD metal oxide coatings were prepared using a slurry casting method on Al foil current collectors. To prepare the slurry, MCN microflakes, acetylene black, and polyvinylidene fluoride were mixed in a weight ratio of 70:20:10, respectively, in *N*-methyl pyrrolidin-2-one solvent. The slurry was then coated on the Al foil and dried at 90 °C overnight.

Al_2O_3, ZrO_2, and TiO_2 thin films were directly coated on the MCN electrodes in a Savannah 100 ALD system (Cambridge Nanotechnology Inc., USA). Trimethylaluminum, tetrakis dimethylamido zirconium ($Zr(NMe_2)_4$), and titanium tetraisopropoxide were used as Al, Zr, and Ti precursor, respectively, while H_2O acted as an oxidizer. The deposition temperature for Al_2O_3, ZrO_2 was 100 °C, while TiO_2 was deposited at 85 °C. The number of ALD cycles was fixed as 2 for all three types of coatings. A complete procedure for ALD coatings can be found in the previous work.[22,25,27,53] Al_2O_3 deposited with 10 ALD cycles was also performed for surface morphological characterization. Pristine, Al_2O_3, ZrO_2, and TiO_2 coated with 2 ALD cycles on MCN electrode were labeled as MCN, MCN–Al, MCN–Zr, and MCN–Ti, respectively. The different metal oxide coatings with 2 ALD cycles on the MCN powders were also completed for physical property measurements.

Physical and Electrochemical Characterization: XRD patterns of pristine and MCN coated with different metal oxides were measured by using a Bruker D8 Discover Diffractometer equipped with a K_α radiation source (λ = 1.5406 nm). Surface morphology of the powders was observed using a HR-TEM (JEOL 2010 FEG) and field emission scanning electron microscope (SEM, Hitachi S-4800) coupled with an energy dispersive spectrometer. The existence of metal oxides on MCN electrode was confirmed by synchrotron-based XPS recorded on the variable line spacing plane grating monochromator (VLS PGM) beamline at the Canadian Light Source (CLS), Saskatchewan in Saskatoon. XAFS data were collected at the CLS using an 06ID superconducting wiggler sourced hard X-ray microanalysis beamline with a premirror—double crystal monochromator—postmirror configuration by Si (111) crystals and Rh mirrors. Energy calibration was conducted using Co, Ni, and Mn foil at their corresponding edges. Beamline current and wiggler were running at 250 mA and 1.9 T, respectively. All XAFS measurements were taken at room temperature in transmission and fluorescence mode using a 32 element Ge detector.

CR2032 coin-type cell configuration was used to test electrochemical performance of the obtained electrodes. Electrodes, with a size of 1 cm^2, were punched out from the slurry coated Al foil for the cell fabrication. The cells were fabricated in an argon filled glove box by pressing a cathode (MCN or MCN–Al or MCN–Zr or MCN–Ti), polypropylene separator (Celgard 2400), and sodium foil anode together. The electrolyte used in the present investigation was 1 M $NaClO_4$ in ethylene carbonate and diethyl carbonate (1:1; v/v). The charge–discharge experiments were carried out within a potential range of 2–4.5 V at various current densities (0.16 A g^{-1} = 1 C) in an Arbin BT-2000 testing station. EIS and CV were conducted using an electrochemical analyzer (SP-150, Bio-Logic, France). All experiments were conducted at room temperature.

Supporting Information

Supporting Information is available from the Wiley Online Library or from the author.

Acknowledgements

This research was supported by the Natural Sciences and Engineering Research Council of Canada (NSERC), the Canada Research Chair (CRC) Program, the Canada Foundation for Innovation (CFI), the Ontario Research Fund (ORF), the Canadian Light Source (CLS), the McMaster National Microscopy Centre, the University of Western Ontario, and the National Natural Science Foundation of China (NSFC) (grant no. 51672189). K.K. was supported by the MITACS.

Conflict of Interest

The authors declare no conflict of interest.

Keywords

atomic layer deposition, high rates, metal oxides, P2-type, sodium-ion batteries

Received: April 7, 2017
Revised: June 19, 2017
Published online: August 7, 2017

[1] M. Armand, J. M. Tarascon, *Nature* **2008**, *451*, 652.
[2] M. D. Slater, D. Kim, E. Lee, C. S. Johnson, *Adv. Funct. Mater.* **2013**, *23*, 947.
[3] V. Palomares, P. Serras, I. Villaluenga, K. B. Hueso, J. Carretero-Gonzalez, T. Rojo, *Energy Environ. Sci.* **2012**, *5*, 5884.
[4] S.-W. Kim, D.-H. Seo, X. Ma, G. Ceder, K. Kang, *Adv. Energy Mater.* **2012**, *2*, 710.
[5] S. Miyazaki, S. Kikkawa, M. Koizumi, *Synth. Met.* **1983**, *6*, 211.
[6] S. Kikkawa, S. Miyazaki, M. Koizumi, *J. Power Sources* **1985**, *14*, 231.
[7] H. Yoshida, N. Yabuuchi, S. Komaba, *Electrochem. Commun.* **2013**, *34*, 60.
[8] M. Sathiya, K. Hemalatha, K. Ramesha, J. M. Tarascon, A. S. Prakash, *Chem. Mater.* **2012**, *24*, 1846.
[9] A. Gupta, C. Buddie Mullins, J. B. Goodenough, *J. Power Sources* **2013**, *243*, 817.
[10] M. Guignard, C. Didier, J. Darriet, P. Bordet, E. Elkaïm, C. Delmas, *Nat. Mater.* **2013**, *12*, 74.
[11] J.-J. Ding, Y.-N. Zhou, Q. Sun, Z.-W. Fu, *Electrochem. Commun.* **2012**, *22*, 85.
[12] K. Chihara, A. Kitajou, I. D. Gocheva, S. Okada, J.-I. Yamaki, *J. Power Sources* **2013**, *227*, 80.

[13] D. Yuan, X. Hu, J. Qian, F. Pei, F. Wu, R. Mao, X. Ai, H. Yang, Y. Cao, *Electrochim. Acta* **2014**, *116*, 300.
[14] H. Yoshida, N. Yabuuchi, K. Kubota, I. Ikeuchi, A. Garsuch, M. Schulz-Dobrick, S. Komaba, *Chem. Commun.* **2014**, *50*, 3677.
[15] H. Yu, S. Guo, Y. Zhu, M. Ishida, H. Zhou, *Chem. Commun.* **2014**, *50*, 457.
[16] N. Yabuuchi, M. Kajiyama, J. Iwatate, H. Nishikawa, S. Hitomi, R. Okuyama, R. Usui, Y. Yamada, S. Komaba, *Nat. Mater.* **2012**, *11*, 512.
[17] P. Barpanda, G. Liu, C. D. Ling, M. Tamaru, M. Avdeev, S.-C. Chung, Y. Yamada, A. Yamada, *Chem. Mater.* **2013**, *25*, 3480.
[18] H. Wang, B. Yang, X.-Z. Liao, J. Xu, D. Yang, Y.-S. He, Z.-F. Ma, *Electrochim. Acta* **2013**, *113*, 200.
[19] K. Park, D. Han, H. Kim, W.-S. Chang, B. Choi, B. Anass, S. Lee, *RSC Adv.* **2014**, *4*, 22798.
[20] Z. Lu, J. R. Dahn, *J. Electrochem. Soc.* **2001**, *148*, A1225.
[21] L. Si, Z. Yuan, L. Hu, Y. Zhu, Y. Qian, *J. Power Sources* **2014**, *272*, 880.
[22] Y. Lu, S. Zhang, Y. Li, L. Xue, G. Xu, X. Zhang, *J. Power Sources* **2014**, *247*, 770.
[23] X. Meng, X.-Q. Yang, X. Sun, *Adv. Mater.* **2012**, *24*, 3589.
[24] X. Li, J. Liu, M. N. Banis, A. Lushington, R. Li, M. Cai, X. Sun, *Energy Environ. Sci.* **2014**, *7*, 768.
[25] X. Li, X. Meng, J. Liu, D. Geng, Y. Zhang, M. N. Banis, Y. Li, J. Yang, R. Li, X. Sun, M. Cai, M. W. Verbrugge, *Adv. Funct. Mater.* **2012**, *22*, 1647.
[26] X. Li, J. Liu, B. Wang, M. N. Banis, B. Xiao, R. Li, T.-K. Sham, X. Sun, *RSC Adv.* **2014**, *4*, 27126.
[27] X. Li, J. Liu, X. Meng, Y. Tang, M. N. Banis, J. Yang, Y. Hu, R. Li, M. Cai, X. Sun, *J. Power Sources* **2014**, *247*, 57.
[28] J. Cho, Y. J. Kim, B. Park, *Chem. Mater.* **2000**, *12*, 3788.
[29] S. Amaresh, K. Karthikeyan, K. J. Kim, M. C. Kim, K. Y. Chung, B. W. Cho, Y. S. Lee, *J. Power Sources* **2013**, *244*, 395.
[30] X. Han, Y. Liu, Z. Jia, Y.-C. Chen, J. Wan, N. Weadock, K. J. Gaskell, T. Li, L. Hu, *Nano Lett.* **2013**, *14*, 139.
[31] K. Kaliyappan, J. Liu, A. Lushington, R. Li, X. Sun, *ChemSusChem* **2015**, *8*, 2537.
[32] K. Karthikeyan, S. Amaresh, G. W. Lee, V. Aravindan, H. Kim, K. S. Kang, W. S. Kim, Y. S. Lee, *Electrochim. Acta* **2012**, *68*, 246.
[33] K. Karthikeyan, S. Amaresh, S. H. Kim, V. Aravindan, Y. S. Lee, *Electrochim. Acta* **2013**, *108*, 749.
[34] S. R. Whitman, K. S. Raja, *Appl. Surf. Sci.* **2014**, *303*, 406.
[35] K. N. Chappanda, Y. R. Smith, L. W. Rieth, P. Tathireddy, M. Misra, S. K. Mohanty, *J. Electrochem. Soc.* **2014**, *161*, H431.
[36] D. Yuan, W. He, F. Pei, F. Wu, Y. Wu, J. Qian, Y. Cao, X. Ai, H. Yang, *J. Mater. Chem. A* **2013**, *1*, 3895.
[37] J. Li, M. Fan, X. He, R. Zhao, C. Jiange, C. Wan, *Ionics* **2006**, *12*, 215.
[38] P. Samarasingha, D.-H. Tran-Nguyen, M. Behm, A. Wijayasinghe, *Electrochim. Acta* **2008**, *53*, 7995.
[39] Y. J. Kim, J. Cho, T.-J. Kim, B. Park, *J. Electrochem. Soc.* **2003**, *150*, A1723.
[40] J. M. Zheng, J. Li, Z. R. Zhang, X. J. Guo, Y. Yang, *Solid State Ionics* **2008**, *179*, 1794.
[41] C. Li, H. P. Zhang, L. J. Fu, H. Liu, Y. P. Wu, E. Rahm, R. Holze, H. Q. Wu, *Electrochim. Acta* **2006**, *51*, 3872.
[42] H.-M. Cheng, F.-M. Wang, J. P. Chu, R. Santhanam, J. Rick, S.-C. Lo, *J. Phys. Chem. C* **2012**, *116*, 7629.
[43] V. V. Afanas'ev, M. Houssa, A. Stesmans, M. M. Heyns, *J. Appl. Phys.* **2002**, *91*, 3079.
[44] J. Cho, Y. J. Kim, T.-J. Kim, B. Park, *Angew. Chem. Int. Ed.* **2001**, *40*, 3367.
[45] K. Ado, M. Tabuchi, H. Kobayashi, H. Kageyama, O. Nakamura, Y. Inaba, R. Kanno, M. Takagi, Y. Takeda, *J. Electrochem. Soc.* **1997**, *144*, L177.
[46] W.-S. Yoon, C. P. Grey, M. Balasubramanian, X.-Q. Yang, J. McBreen, *Chem. Mater.* **2003**, *15*, 3161.
[47] M. G. Kim, C. H. Yo, *J. Phys. Chem. B* **1999**, *103*, 6457.
[48] M. G. Kim, H. J. Shin, J.-H. Kim, S.-H. Park, Y.-K. Sun, *J. Electrochem. Soc.* **2005**, *152*, A1320.
[49] D. Buchholz, L. G. Chagas, M. Winter, S. Passerini, *Electrochim. Acta* **2013**, *110*, 208.
[50] X. Ma, H. Chen, G. Ceder, *J. Electrochem. Soc.* **2011**, *158*, A1307.
[51] X. Chen, X. Zhou, M. Hu, J. Liang, D. Wu, J. Wei, Z. Zhou, *J. Mater. Chem. A* **2015**, *3*, 20708.
[52] Y. Zhu, X. Qi, X. Chen, X. Zhou, X. Zhang, J. Wei, Y. Hub, Z. Zhou, *J. Mater. Chem. A* **2016**, *4*, 11103.
[53] J. Liu, M. N. Banis, X. Li, A. Lushington, M. Cai, R. Li, T.-K. Sham, X. Sun, *J. Phys. Chem. C* **2013**, *117*, 20260.